Journal of Power Sources 267 (2014) 69–77

Contents lists available at ScienceDirect

Journal of Power Sources

journal homepage: www.elsevier.com/locate/jpowsour

Enhanced hydrogen storage properties of magnesium by the synergic catalytic effect of $TiH_{1.971}$ and $TiH_{1.5}$ nanoparticles at room temperature

Tong Liu [a, *], Chunguang Chen [a], Fan Wang [a], Xingguo Li [b]

[a] Key Laboratory of Aerospace Materials and Performance (Ministry of Education), School of Materials Science and Engineering, Beihang University, Beijing 100191, China

[b] Beijing National Laboratory for Molecular Sciences (BNLMS), The State Key Laboratory of Rare Earth Materials Chemistry and Applications, College of Chemistry and Molecular Engineering, Peking University, Beijing 100871, China

HIGHLIGHTS

- The Mg–9.2wt%$TiH_{1.971}$–3.7wt% $TiH_{1.5}$ nanocomposite was prepared.
- The Ti hydrides nanoparticles of 13 nm were dispersed on the Mg nanoparticles.
- $TiH_{1.971}$ and $TiH_{1.5}$ nanoparticles cooperatively catalyzed the hydrogenation of Mg.
- The nanocomposite absorbed 4.3 wt% H_2 in 10 min at room temperature.
- The apparent activation energy for hydrogen absorption was 12.5 kJ mol^{-1}.

GRAPHICAL ABSTRACT

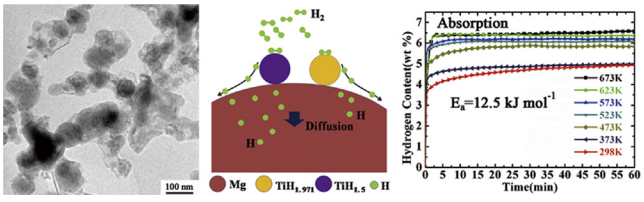

ARTICLE INFO

Article history:
Received 27 February 2014
Received in revised form
29 April 2014
Accepted 12 May 2014
Available online 20 May 2014

Keywords:
Magnesium
Titanium hydride
Nanocomposite
Hydrogen storage
Kinetics

ABSTRACT

In order to improve the hydrogen sorption kinetics of Mg at room temperature, the Mg–9.2wt%$TiH_{1.971}$–3.7wt%$TiH_{1.5}$ nanocomposite is successfully prepared by hydrogen plasma-metal reaction (HPMR) method and hydrogenation/dehydrogenation at 673 K. The Mg nanoparticles are hexagonal in shape with the size in the range of 50–190 nm. The spherical Ti hydrides nanoparticles of about 13 nm are uniformly dispersed on the surface of Mg nanoparticles. During hydrogenation/dehydrogenation cycle, the Ti hydrides nanoparticles restrain the growth of Mg nanoparticles. The Mg–$TiH_{1.971}$–$TiH_{1.5}$ nanocomposite quickly absorbs 4.3 wt% H_2 in 10 min at room temperature and reaches a saturation value of 5.0 wt% in 60 min. The apparent activation energies for hydrogen absorption and desorption are 12.5 and 46.2 kJ mol^{-1}, respectively. The improved kinetics and reduced activation energy are explained in terms of the nanostructure of Mg and the synergic catalytic effect of $TiH_{1.971}$–$TiH_{1.5}$ nanoparticles.

1. Introduction

Hydrogen, because of its high energy density and pollution-free properties, is good energy carrier alternative to conventional fossil fuels for future automotives. However, the wide-ranging application of hydrogen is still challenged by its storage technology [1]. Metal hydrides are considered as the most potential candidate for

* Corresponding author. Tel./fax: +86 10 8231 6192.
E-mail address: tongliu@buaa.edu.cn (T. Liu).

http://dx.doi.org/10.1016/j.jpowsour.2014.05.066
0378-7753/

hydrogen storage materials due to their superior properties in storage capacity and safety [2]. Among metal hydrides, MgH_2 is still the most attractive due to its high theoretical gravimetric capacity of 7.6 wt% H_2, reversibility, abundance and low cost. Nevertheless, some thresholds still lie in both thermodynamic and kinetic properties for the practical application of MgH_2 [3]. Typically, the hydrogenation of Mg needs a temperature higher than 573 K and the dehydrogenation temperature is even higher due to the high thermodynamic stability of MgH_2 (decomposition enthalpy of MgH_2 is 75 kJ mol^{-1} H_2) [4,5]. At room temperature, the hydrogen sorption rate is rather low due to poor kinetics [6]. Therefore, it is important to lower the operation temperature and improve the sorption kinetics in the meantime.

The addition of catalyst is an effective way to improve the sorption kinetics of Mg hydride. Recent works indicate that doping a small percentage of catalytic 3d-transition metals, such as Ti, V, Mn, Fe, Ni, Co and Cu can intensively enhance the sorption kinetics of Mg without apparently reducing its high hydrogen capacity [7–11]. High energy ball milling (HEBM) is the most common method to disperse additives in Mg. Liang and coworkers found that the MgH_2 + 5 at% V composites prepared by ball milling absorbed 5 wt% H_2 at 423 K in 10 min [10]. It was also found that the ball-milled Mg–Co alloys with body-centered cubic structure (BCC) absorbed 2.1 mass% H_2 at 323 K [11]. As a catalyst, Ti-hydride shows remarkable performance in improving the hydrogen storage properties of Mg, especially at moderate temperatures (<573 K). Cuevas et al. found that during the milling of the Mg–Ti composite under hydrogen atmosphere (8 MPa), the TiH_2 (<15 min) was firstly generated, and the transformation of MgH_2 was followed after [2]. The $7MgH_2/TiH_2$ mixture produced by high-energy-high-pressure (HEHP) mechanical ball-milling started to release H_2 at 399 K [12]. Shao et al. reported that the Mg and Ti composites prepared by milling under hydrogen could even absorb hydrogen at 313 K [13]. Lu and coworkers reported that the milled MgH_2–$0.1TiH_2$ particles could uptake about 4.5 wt % H_2 in 4 h at room temperature under 6 MPa hydrogen pressure [14]. Although moderate operation temperature and high absorption capacity have been achieved in these studies, the hydrogenation rate was still low. Moreover, titanium hydrides, besides TiH_2, contain many kinds of phases, such as $TiH_{1.971}$, $TiH_{1.924}$, $TiH_{1.5}$, TiH and $TiH_{0.71}$ [13–15]. There are some works revealing the catalytic function of TiH_2, but the combining catalytic effect of multiple Ti hydrides in the Mg-based hydrogen storage materials has not been investigated yet. It should be noted that during the ball milling the contamination often induces poor repeatability and difficulties in interpreting the hydrogenation/dehydrogenation mechanism. Meanwhile, recent studies have suggested that when the particle size of Mg is reduced to nanoscale, both the hydrogen absorption and desorption kinetics can be significantly improved [16–21]. Although the grains of the Mg-based particles produced by the HEBM can achieve nanosize, their particle sizes are still in the range of micrometer [11,14]. Thus, it is necessary to improve the sorption kinetics of Mg via using particles in nanoscale and doping novel catalysts.

Hydrogen plasma-metal reaction (HPMR) method is a novel vapor deposition process and suitable for producing metallic nanoparticles industrially with high purity and low cost. Previously, we have demonstrated that HPMR method can be utilized to prepare Mg-based nanocomposites with enhanced hydrogen storage properties, such as Mg–Al and Mg–V [22,23]. In this work, we intend to produce Mg–$TiH_{1.971}$–$TiH_{1.5}$ nanocomposite by HPMR and hydrogenation/dehydrogenation at 673 K, investigate their hydrogen storage properties at room temperature, and clarify the synergic catalytic effect of two kinds of Ti hydrides nanoparticles.

2. Experimental

The equipment for producing nanoparticles primarily contains an arc melting chamber and a collecting system, which was described elsewhere [24]. The Mg-based nanocomposite were produced by arc melting Mg (purity >99.9%) ingot of 22 g and Ti (purity >99.9%) ingot of 14 g in a 50% Ar and 50% H_2 mixture of 0.1 MPa. The arc current was selected as 150 A. The flow rate of the circulation gas for the collection of nanoparticles was 100 L min^{-1}. Before the nanoparticles were taken out from the collection room, they were passivated with a mixture of argon and air to prevent the particles from burning. The Mg and $TiH_{1.971}$ nanoparticles were also synthesized by the HPMR method at the same condition with the Mg-based nanocomposite, respectively.

The hydrogen desorption and absorption properties were evaluated using a Sieverts-type apparatus. The volume of the reactor chamber was about 60 ml, and the error of the measurement was less than 5%. To obtain the Mg–$TiH_{1.971}$–$TiH_{1.5}$ nanocomposite, the as-prepared Mg-based nanocomposite of 100 mg was heated to 673 K to experience one hydrogen absorption/desorption cycle in hydrogen (4 MPa) and vacuum. To measure the absorption kinetic curves, the system was evacuated to 10^{-3} Pa, and the samples were heated up to 298, 373, 473, 523, 573, 623 and 673 K, respectively. A hydrogen pressure of 4 MPa was provided to make the Mg–Ti hydrides nanocomposite absorb hydrogen. The desorption kinetic curves at various temperatures were measured at an initial pressure of about 100 Pa by evacuating the system. A conventional pressure–volume–temperature technique was used to obtain the hydrogen sorption curves and pressure–composition (P–C) isotherm curves at different temperatures. Once the change of hydrogen pressure was less than 20 Pa s^{-1}, the hydrogen absorption or desorption process at certain pressure was considered as reaching equilibrium during the P–C isotherm measurement. The hydrogen sorption properties of $TiH_{1.971}$ nanoparticles were also measured at the same condition as the Mg–Ti hydrides nanocomposite. Before the measurement, the samples experienced one hydrogenation/dehydrogenation cycle, similar with the Mg–Ti hydrides nanocomposite.

The structural analyses of the Mg–Ti hydrides nanocomposite before and after the hydrogen sorption were carried out by X-ray diffraction (XRD) using a Rigaku X-ray diffractometer with monochromatic Cu Ka radiation. The morphology, size distribution and shape of the nanoparticle samples were observed by transmission electron microscope (TEM) using JEOL-JSM-2100 at an accelerating voltage of 200 kV. For comparison, the structural and morphology analyses of the Mg nanoparticles were also conducted by XRD and TEM. The energy dispersive X-ray spectroscopy (EDX) was used to determine the contents of Mg and Ti in the nanocomposite.

3. Results and discussion

3.1. Particle features

Fig. 1(a) displays the TEM image of the as-prepared Mg-based nanocomposite by HPMR method, and the inset figure is the histograms of size distribution. It can be seen that there are two types of particles. The big particles vary from 40 to 180 nm with an average of about 115 nm. They have clear hexagonal shapes, which are the same as the pure Mg ultrafine particles prepared by HPMR [25]. Compared with the Mg nanoparticles of about 300 nm (see Fig. S1) in average prepared by HPMR, the addition of Ti greatly reduces the particle size of Mg. Fig. 1(b) displays the high resolution TEM image of one big particle. The interplanar spacing is measured to be 2.780 Å, corresponding to the Mg (100), 2.778 Å. It demonstrates that the big particles are Mg. On the surface of each big

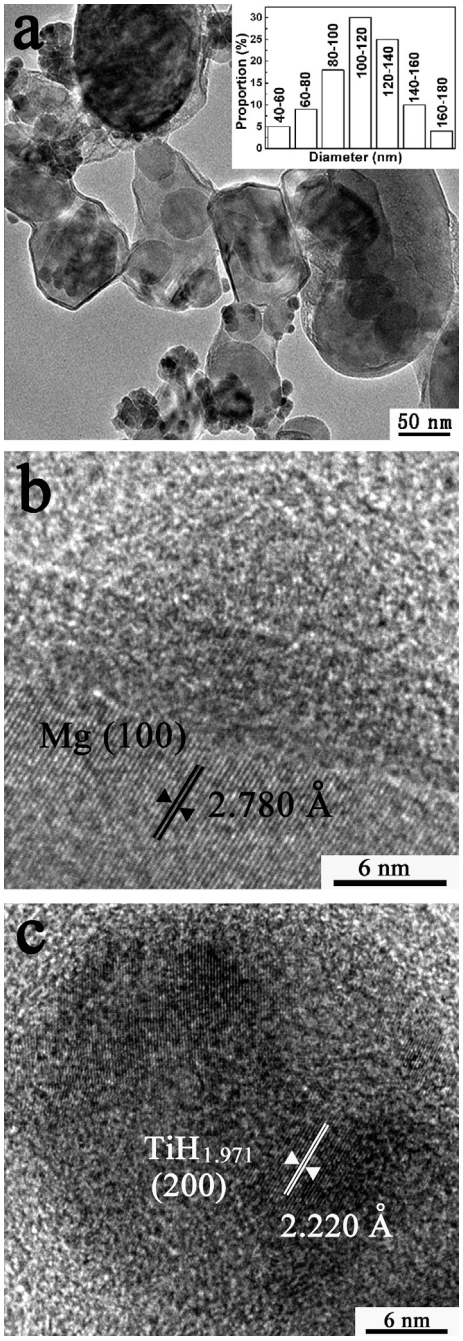

Fig. 1. TEM bright-field image of the as-prepared Mg-$TiH_{1.971}$ nanocomposite (a), HR-TEM image of Mg (b) and HR-TEM image of $TiH_{1.971}$ (c).

particle, the small spherical particles of about 13 nm are dispersed uniformly. Fig. 1(c) displays the high resolution TEM image of a small particle. The interplanar spacing of the small particle is 2.220 Å, which belongs to the (200) of $TiH_{1.971}$, 2.221 Å. The EDS result in Fig. 2 displays that the average Ti content in the Mg–$TiH_{1.971}$ nanocomposite is 12.4 wt%. Therefore, the as-prepared nanocomposite synthesized by HPMR is Mg–12.9wt%$TiH_{1.971}$. The lower Ti content in the as-prepared nanoparticles than that in the master ingot is due to the higher evaporation rate of Mg than that of Ti in the HPMR process.

Fig. 3 shows the XRD patterns of the as-prepared Mg-based nanocomposite, the samples obtained after hydrogenation/dehydrogenation cycle at 673 K and after the hydrogen absorption at

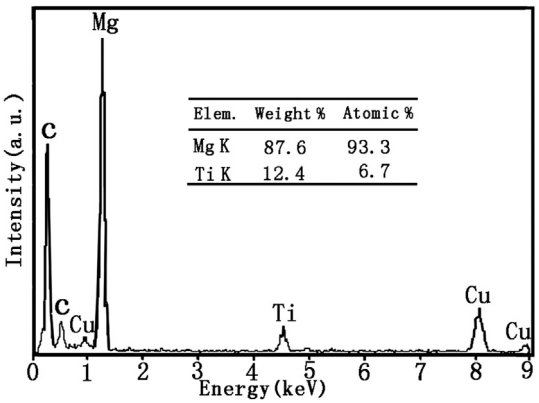

Fig. 2. The energy dispersive X-ray spectroscopy of the Mg-$TiH_{1.971}$ nanocomposite.

room temperature. It is found in Fig. 3(a) that the as-prepared Mg-based nanocomposite contains dominantly α-Mg (hcp) together with a certain amount of $TiH_{1.971}$, in good agreement with the TEM observation (Fig. 1). No diffraction peaks of MgH_2 are found due to the poor formation kinetics and thermodynamics of MgH_2. The lattice constants of Mg calculated from the XRD data are $a = 3.209$ Å and $c = 5.210$ Å, the same as the standard data of pure α-Mg (JCPDS 35-0821). This indicates that no Ti dissolves in Mg, in good agreement with the Mg–Ti equilibrium binary diagram [15]. It is worth to note that the diffraction peak of MgO around 42.9°, which usually appears in the Mg particles prepared by HPMR (see Fig. S2), cannot be detected in the present XRD pattern of the as-prepared nanoparticles. This demonstrates that the addition of Ti effectively suppresses the pyrophoricity of Mg, and decreases the MgO content in the nanoparticles after the passivation process. It is shown in Fig. 3(b) that after the hydrogenation/dehydrogenation cycle at 673 K, MgH_2 dehydrogenates and changes completely into α-Mg. From the XRD pattern in Fig. 3(c), it can be found that after the absorption process at room temperature, most of the Mg in Mg-based nanocomposite transforms into MgH_2. But, a little amount of Mg still exists due to the insufficient hydrogenation at such low temperature. The peak of MgO at 42.9° is detectable in both Fig. 3(b) and (c), which is attributed to the fact that the nanoparticles are taken out of the chamber without sufficient passivation after the absorption and desorption processes. It has been reported that $TiH_{1.971}$ can decompose to $TiH_{1.5}$ during the dehydrogenation process at around 673 K [26–28]. Analyzed from the XRD result of the Mg-based nanocomposite in Fig. 3(b) and (c), however, $TiH_{1.5}$ phase cannot be identified, probably due to its low content.

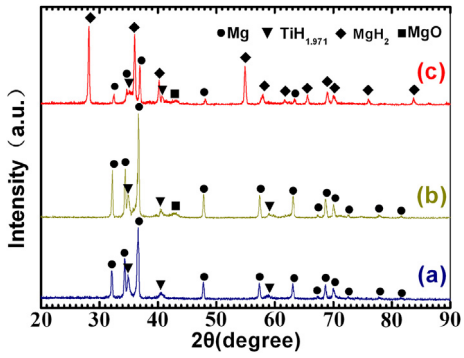

Fig. 3. XRD patterns of the as-prepared Mg-based nanocomposite by HPMR (a), after hydrogenation/dehydrogenation at 673 K (b) and after the absorption under 4 MPa hydrogen pressure at 298 K (c).

In order to clarify the evolution of $TiH_{1.971}$ in the Mg–Ti hydrides nanocomposite during the hydrogenation/dehydrogenation cycle, the $TiH_{1.971}$ nanoparticles have been synthesized by HPMR method at the same condition with the Mg–$TiH_{1.971}$ nanocomposite. The $TiH_{1.971}$ nanoparticles have the similar particle size with those in the Mg–$TiH_{1.971}$ nanocomposite of about 13 nm, as shown in Fig. 4(a). The measured lattice fringe spacing is 2.603 Å, corresponding to (111) plane of $TiH_{1.971}$ (see Fig. 4(b)). The XRD patterns of the as-prepared $TiH_{1.971}$, after hydrogenation/dehydrogenation at 673 K and after hydrogenation at room temperature are shown in Fig. 5. It is observed in Fig. 5(a) that the as-prepared sample is made of $TiH_{1.971}$, and no other phases can be detected. It also implies that the Mg-based nanocomposite prepared by HPMR contains merely Mg and $TiH_{1.971}$. After hydrogenation/dehydrogenation at 673 K, the peaks of $TiH_{1.5}$ at 35.1, 39.3 and 40.3° can be detected in Fig. 5(b), which is the same as the reported works [27]. The lattice parameter calculated from (111) and (002) reflections of $TiH_{1.5}$ is 4.43 Å, similar with other studies [27,28]. It demonstrates that in the present work a certain amount of $TiH_{1.971}$ decomposes to $TiH_{1.5}$ during the dehydrogenation at 673 K. Therefore, the initial state of the Mg–Ti hydrides nanocomposite before hydrogenation measurement is the Mg–$TiH_{1.971}$–$TiH_{1.5}$ nanocomposite. According to the XRD peak intensities of $TiH_{1.971}$ and $TiH_{1.5}$, the mass ratio of $TiH_{1.971}$ to $TiH_{1.5}$ is estimated to be 2.5:1. Then, the nanocomposite can be referred to as Mg–9.2wt% $TiH_{1.971}$–3.7wt% $TiH_{1.5}$. After hydrogenation at room temperature, a certain amount of $TiH_{1.5}$ is still detectable due to its low hydrogenation rate at such low temperature, see Fig. 5(c). However, the diffraction peak intensity ratio of $TiH_{1.971}$ to $TiH_{1.5}$ becomes larger, implying the transformation of $TiH_{1.5}$ to $TiH_{1.971}$.

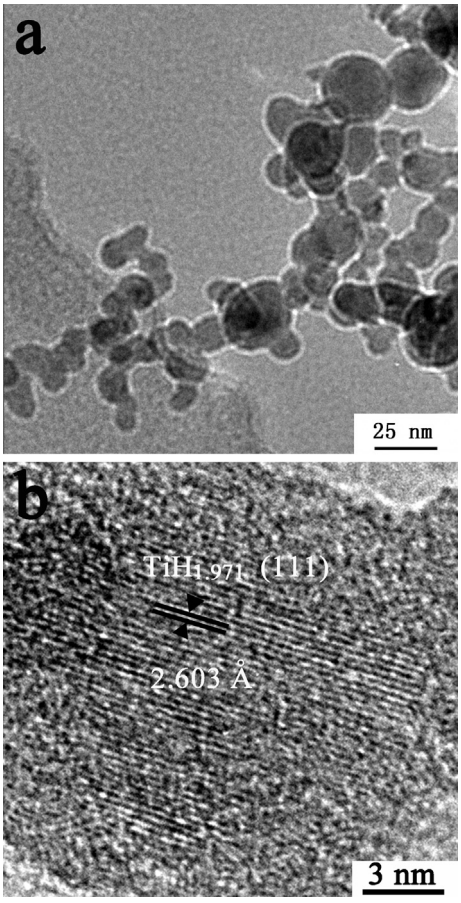

Fig. 4. TEM bright-field image (a) and HR-TEM image (b) of the as-prepared $TiH_{1.971}$ nanoparticles.

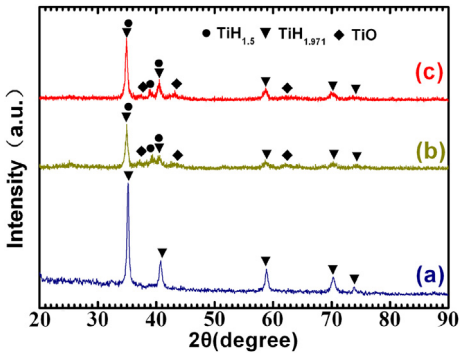

Fig. 5. XRD patterns of the $TiH_{1.971}$ nanoparticles (a) and the samples after hydrogenation/dehydrogenation at 673 K (b) and after hydrogenation at room temperature (c).

Fig. 6 shows the TEM and HR-TEM images of Mg-$TiH_{1.971}$ nanocomposite after the hydrogenation/dehydrogenation process at 673 K. From Fig. 6(a), it is observed that the particle morphology and size does not apparently change after the hydrogenation/dehydrogenation. The big particles possess polyhedral shape, and the particle size varies from 50 to 190 nm, about 125 nm in average. In this work, $TiH_{1.971}$–$TiH_{1.5}$ nanoparticles act as a strong size control conductor during the hydrogenation/dehydrogenation cycle, similar with the effect of TiH_2 [26]. Fig. 6(c) displays the HR-TEM image of the selected zone 1 in Fig. 6(b). It is worth to note that, for the big particle, the measured lattice fringe spacing is 2.800 Å, corresponding to (100) plane of hcp-Mg, and no fringe of MgH_2 can be observed. This proves that MgH_2 dehydrogenates completely into α-Mg, in agreement with the XRD result (Fig. 3(b)). Fig. 6(d) displays the HR-TEM image of the selected zone 2 in Fig. 6(b). The lattice fringes with a spacing of 2.590 Å belongs to (111) plane of $TiH_{1.971}$.

Fig. 7 presents the TEM and HR-TEM images of the Mg–$TiH_{1.971}$–$TiH_{1.5}$ nanocomposite after hydrogen absorption at room temperature. It can be seen clearly that the particles keep polyhedral shape, and the particle size varies from 60 to 210 nm with an average of about 130 nm, as shown in Fig. 7(a). The small particles are also homogeneously distributed on the surfaces of the large particles. Fig. 7(c) displays the HR-TEM image of the selected zone 1 in Fig. 7(b). It is worth of pointing that there are two kinds of lattice fringes in the big particle. One kind of lattice fringe corresponds to MgH_2 (112) with a spacing of 2.076 Å, and the other with a spacing of 1.905 Å belongs to (102) plane of hcp-Mg. The existence of a small amount of Mg is due to the insufficient hydrogenation at such low temperature, in well agreement with the XRD result in Fig. 3(c). Fig. 7(d) displays the HR-TEM image of the selected zone 2 in Fig. 7(b). The fine black particles are determined as $TiH_{1.971}$ and keep similar particle size of about 13 nm as in the as-prepared nanocomposite.

On the basis of the analysis above, the HPMR, the hydrogenation and dehydrogenation processes of the Mg–Ti hydrides nanocomposite can be summarized into the following equations, respectively.

$$Mg + Ti + H_2 \rightarrow Mg + TiH_{1.971} \quad (1)$$

$$Mg + TiH_{1.5} + TiH_{1.971} + H_2 \rightarrow MgH_2 + TiH_{1.5} + TiH_{1.971} \quad (2)$$

$$MgH_2 + TiH_{1.5} + TiH_{1.971} \rightarrow Mg + TiH_{1.5} + TiH_{1.971} + H_2 \quad (3)$$

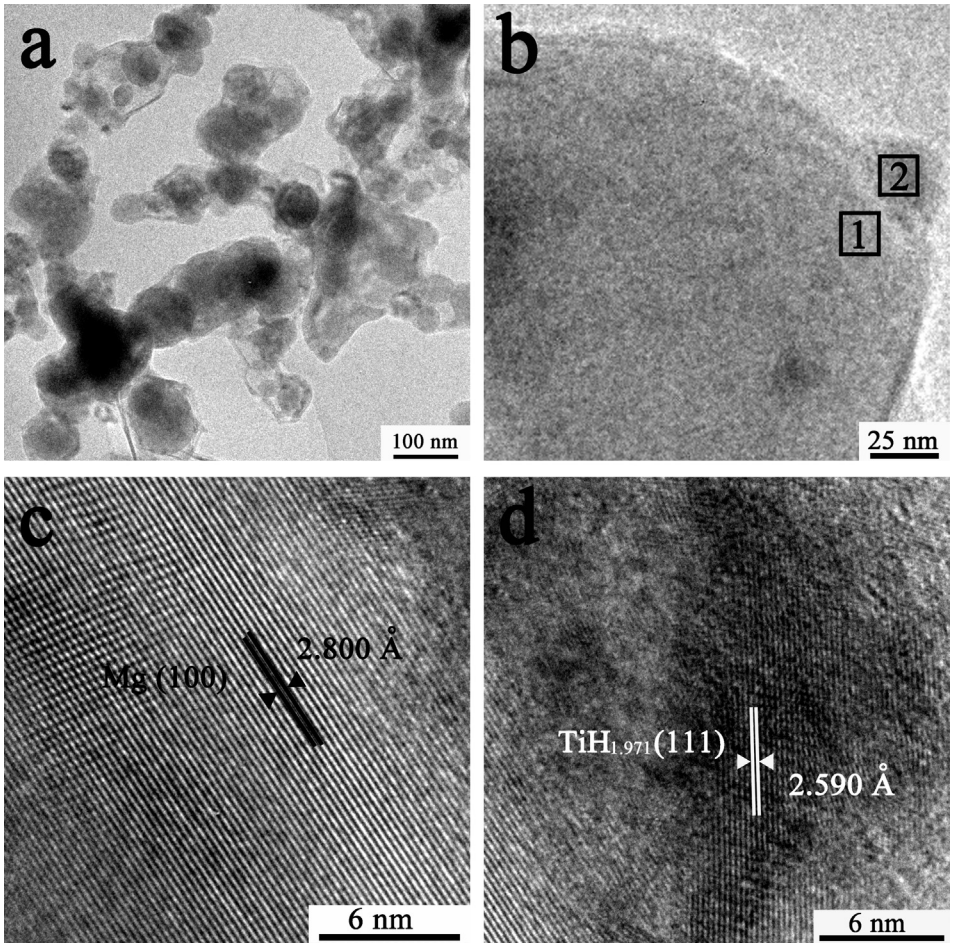

Fig. 6. TEM bright-field images of Mg–$TiH_{1.971}$ nanocomposite after the hydrogenation/dehydrogenation process at 673 K (a), at high magnification (b), HR-TEM image of one big particle (c) and HR-TEM image of a small nanoparticle on the big particle (d).

3.2. Hydrogen storage properties

The activation treatment through annealing at 673 K in vacuum and in hydrogen for several cycles is often required for the micro-size Mg particles [29]. However, even after this activation process, Mg at microscale can absorb only 1.5 wt% H_2 within 2 h at 673 K [29,30]. The hydrogen absorption curves of the Mg–$TiH_{1.971}$–$TiH_{1.5}$ nanocomposite at different temperatures under 4 MPa are plotted in Fig. 8(a). It is surprisingly observed that the hydrogenation performance of the Mg–$TiH_{1.971}$–$TiH_{1.5}$ nanocomposite at room temperature is remarkable. The nanocomposite can quickly uptake 4.3 wt% H_2 in 10 min at room temperature and reach a value of 5.0 wt% in 60 min. Lu et al. reported that the ball-milled MgH_2–0.1TiH_2 particles absorbed about 3.5 wt% H_2 in 4 h under the hydrogen pressure of 4 MPa at room temperature [14]. This indicates that the nanosized particles of Mg–Ti hydrides are superior to the micrometer level particles of Mg–TiH_2 with respect to the hydrogenation properties at room temperature. Meanwhile, the synergic catalytic effect of $TiH_{1.971}$–$TiH_{1.5}$ nanoparticles is more effective than TiH_2 alone. To the best of our knowledge, this is the best hydrogenation performance for the Mg-based particles at room temperature.

It is also found in Fig. 8(a) that all the curves exhibit fast initial hydrogen absorption rates. For example, the nanocomposite can quickly absorb hydrogen at 373 K and reach a value of 4.6 wt% H_2 in 5 min. Shao et al. reported that it took more than 4 h for the ball-milled Mg and Ti composite to absorb 4.0 wt% H_2 at 373 K [13]. In this work, the nanocomposite also can quickly absorb hydrogen at 473 K and reach a value of 5.8 wt% H_2 in 60 min, superior to the very recent report that Mg nanoparticles with a mean particle size of 25 nm could absorb nearly 5 wt% at 493 K [31]. The nanocomposite can quickly absorb 6.1 wt% H_2 in 5 min at 573. The Mg nanoparticles synthesized by HPMR method can only uptake 4.7 wt% in 10 min at 573 K (see Fig. S3(a)). The theoretical hydrogenation gravimetric capacity of the Mg–$TiH_{1.971}$–$TiH_{1.5}$ nanocomposite is 6.7 wt%. The storage capacity of the Mg–$TiH_{1.971}$–$TiH_{1.5}$ nanocomposite reaches 6.2 wt% at 573 K, 6.4 wt% at 623 K and 6.7 wt% at 673 K, respectively. Compared with the very recent report that the Mg-polymer nanocomposite had a storage capacity of 4 wt% due to the high percentage of polymer [19], the $TiH_{1.971}$–$TiH_{1.5}$ nanoparticles not only prevent Mg nanoparticles from growing during hydrogenation/dehydrogenation, but also offer the Mg–$TiH_{1.971}$–$TiH_{1.5}$ nanocomposite a high saturation hydrogen storage of 6.7 wt%, reaching the theoretical storage capacity. It can be observed from Fig. 8(b) that the hydrogen desorption rate of the Mg–$TiH_{1.971}$–$TiH_{1.5}$ nanocomposite also increases with the increasing temperature from 473 to 673 K. It should be noted that the nanocomposite can release 6.0 wt% H_2 within 5 min at 623 K, better than the Mg–V system which only desorbs 4.6 wt% H_2 at 623 K [23]. The Mg–$TiH_{1.971}$–$TiH_{1.5}$ nanocomposite can release 3.5 wt% H_2 at 573 K in 5 min, better than the Mg nanoparticles which only desorb 0.8 wt% H_2 in 60 min at the same temperature (see Fig. S3(b)). The hydrogen desorption capacity enlarges remarkably with the increasing temperature. The dehydrogenation

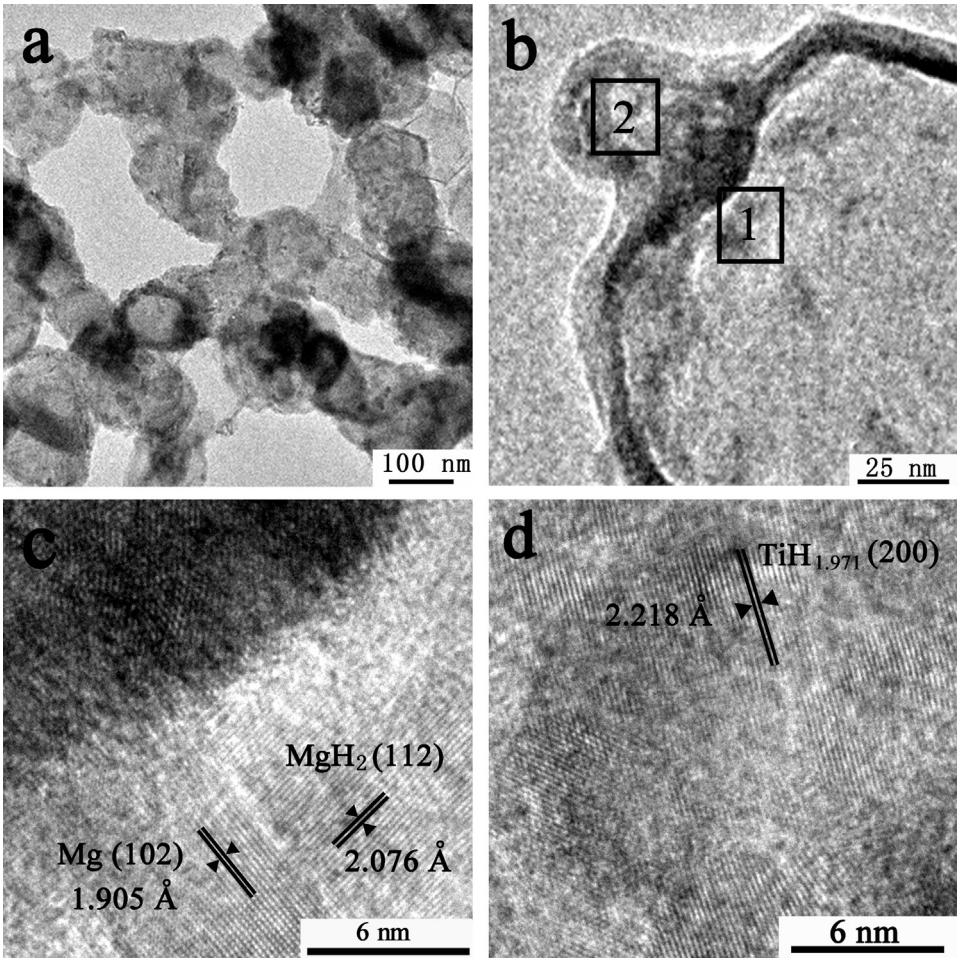

Fig. 7. TEM bright-field images of Mg–$TiH_{1.971}$–$TiH_{1.5}$ nanocomposite after the hydrogen absorption under 4 MPa hydrogen pressure at room temperature (a), at high magnification (b), HR-TEM image of one big particle (c) and HR-TEM image of a small nanoparticle on the big particle (d).

capacity of the nanocomposite reaches 4.1 wt% at 573 K, 6.0 wt% at 623 K and 6.1 wt% at 673 K, respectively.

To clarify the effect of $TiH_{1.971}$–$TiH_{1.5}$ nanoparticles during the hydrogenation/dehydrogenation of Mg-based nanocomposite, the hydrogenation/dehydrogenation curves of the $TiH_{1.971}$–$TiH_{1.5}$ nanoparticles are also measured at 298 and 673 K, see Fig. 9. The nanoparticles can absorb 0.4 wt% H_2 both at room temperature and 673 K, shown in Fig. 9(a). On the basis of the content of Ti in the nanocomposite, the contribution of $TiH_{1.5}$ to the hydrogen absorption value is less than 0.1 wt%. The dehydrogenation curve of the $TiH_{1.971}$–$TiH_{1.5}$ nanoparticles at 673 K is presented in Fig. 9(b) and the hydride nanoparticles release 0.1 wt% H_2 at 673 K, which demonstrates the decomposition of $TiH_{1.971}$. It is found that the $TiH_{1.971}$–$TiH_{1.5}$ nanoparticles almost do not release hydrogen at 100 Pa and 298 K. It should be noted that considering that the Mg-based nanocomposite was heated to 673 K to release hydrogen in vacuum before each hydrogenation measurement, the result that the $TiH_{1.971}$–$TiH_{1.5}$ nanoparticles cannot desorb hydrogen at 100 Pa and 298 K does not influence the catalytic function of these nanoparticles for Mg.

On the basis of JMAK (Johnson–Mehl–Avrami–Kolmogorov) model [32], the hydrogen absorption kinetics can be expressed in the following linear equation:

$$\ln[-\ln(1-\alpha)] = \eta \ln k + \eta \ln t \quad (4)$$

where α is the fraction transformed at time t, k is an effective kinetic parameter namely reaction rate constant, η is the Avrami exponent of reaction order. For the experimental data of 298, 373, 473, 523, 573 and 623 K, by plotting $\ln[-\ln(1-\alpha)]$ vs. $\ln(t)$ (as shown in Fig. 10(a)), each temperature provides a straight line with a slope η and an intercept $\eta\ln(k)$. After calculating the rate constant k from the η value, the apparent activation energy for the absorption process is evaluated from the Arrhenius equation [33,34]:

$$k = A \cdot \exp(-E_a/RT) \quad (5)$$

where E_a represents the activation energy, R is the gas constant (8.314472 J mol^{-1} K^{-1}), and T is the absolute temperature. The absorption plot of $\ln(k)$ vs. $1000/T$ is shown in Fig. 10(c). The calculated hydrogen absorption activation energy of the Mg–$TiH_{1.971}$–$TiH_{1.5}$ nanocomposite is 12.5 kJ mol^{-1}, lower than the MgH_2–0.1TiH_2 particles of 16.4 kJ mol^{-1} and much smaller than that of the 25 nm Mg particles of 122 kJ mol^{-1} [14,31]. By using the same approach, the $\ln[-\ln(1-\alpha)]$ vs. $\ln(t)$ curves for 473, 523, 573 and 623 K are plotted in Fig. 10(b) and the desorption plot of $\ln(k)$ vs. $1000/T$ from the experimental data is shown in Fig. 10(d). The hydrogen desorption activation energy of the Mg–$TiH_{1.971}$–$TiH_{1.5}$ nanocomposite is 46.2 kJ mol^{-1}. This value is also lower than that of the milled MgH_2–0.1TiH_2 particles, 58.4 kJ mol^{-1} [26]. This clearly demonstrates that the $TiH_{1.971}$–$TiH_{1.5}$ nanoparticles efficiently improve the hydrogenation/dehydrogenation rate of Mg. The different values of the reaction order suggest that different mechanisms are controlling the rates at various temperature ranges of absorption. From Fig. 10(a) and (b), we can see that most of the

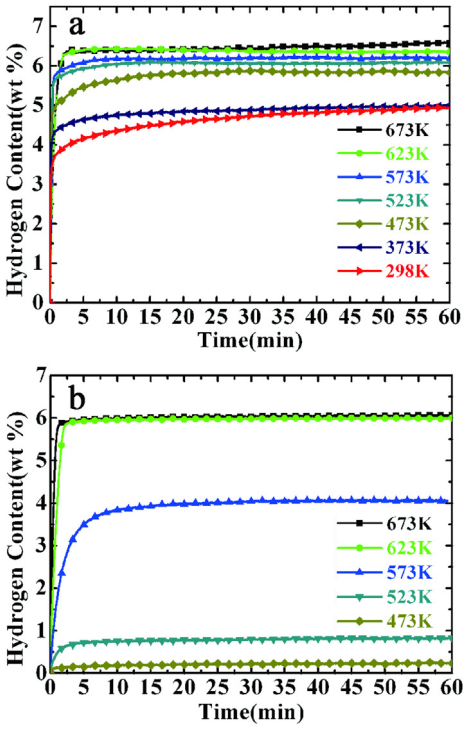

Fig. 8. Hydrogen absorption curves under 4 MPa hydrogen pressure (a) and desorption curves under 100 Pa hydrogen pressure (b) of the Mg–$TiH_{1.971}$–$TiH_{1.5}$ nanocomposite at different temperatures.

reaction order η values at different temperatures are less than 0.5. On the basis of the dependence of η on the growth dimensionality, rate-limiting process, and nucleation behavior reported by Karty et al. [35], it can be concluded that the hydrogenation/dehydrogenation of the Mg–TiH_x nanocomposite is mainly controlled by diffusion-rate limited mechanism and belongs to one-dimensional growth at constant nuclei number. The η value of 1.123 also suggests that the transformation of MgH_2 to Mg upon desorption at 623 K is determined by either diffusion-rate limited occurring by two-dimensional growth at constant nuclei number, or interface-controlled transformation with one-dimensional growth at constant nuclei number.

The enhanced hydrogenation kinetics of Mg can be explained from the following two factors: the nanostructure and the synergic catalytic effect of the $TiH_{1.971}$–$TiH_{1.5}$ nanoparticles. On one hand, the nanostructure of Mg plays an important role in the sorption process. Compared with micro-scale particles, the nanoparticles mean short diffusion distances and also provide more dissociation sites, leading to the enhanced sorption kinetics. However, the effect of the nanostructure alone cannot explain the superior hydrogenation properties at room temperature. On the other hand, the $TiH_{1.971}$–$TiH_{1.5}$ nanoparticles are critical to improve the sorption properties of the Mg-based nanocomposite, especially at room temperature. It is believed that pure Mg without catalytic additives does not have sufficient ability to dissociate hydrogen molecules to enable atomic diffusion inside the particles [36] and shows poor sorption performance (Fig. S3(a)). In the present work, the $TiH_{1.971}$–$TiH_{1.5}$ nanoparticles act as a catalyst to spillover hydrogen to Mg surfaces, decrease the activation energy to dissociate H_2 [37,38]. It is also believed that the oxide layer of Mg particles prevents hydrogen from H transporting into Mg [39]. In this work, the $TiH_{1.971}$–$TiH_{1.5}$ nanoparticles on the surface of Mg decrease the oxide content in the Mg–$TiH_{1.971}$–$TiH_{1.5}$ nanocomposite, which enhances the sorption of H on the surface of the Mg nanoparticles. They also restrain the Mg nanoparticles from growing during hydrogenation/dehydrogenation cycles. More importantly, the $TiH_{1.971}$ nanoparticle, which almost reaches the saturation hydrogenation status, provides active sites for surface adsorption and dissociation, playing the similar role with TiH_2 [26]. Compared with TiH_2, $TiH_{1.5}$ can further absorb a certain amount of hydrogen under suitable condition, which enables them to dissociate hydrogen easily. Prominently, due to the easier hydrogenation of $TiH_{1.5}$ at room temperature (Fig. 9(a)), the initial hydrogenation process of $TiH_{1.5}$ can accelerate the formation of MgH_2, crucial to the hydrogenation of the Mg nanoparticles at room temperature. Thus, the synergic catalytic effect of the $TiH_{1.971}$–$TiH_{1.5}$ nanoparticles is more efficient to improve the sorption kinetics of Mg than TiH_2 alone, illustrated in Fig. 11. In this regards, the reduced activation energy of the nanocomposite is, to a large extent, attributed to the co-existence of $TiH_{1.971}$–$TiH_{1.5}$ nanoparticles.

We further investigate the thermodynamics of the Mg–$TiH_{1.971}$–$TiH_{1.5}$ nanocomposite. Fig. 12(a) shows the *P*–*C*–*T* curves of the hydrogen absorption/desorption for the Mg–$TiH_{1.971}$–$TiH_{1.5}$ nanocomposite at 623, 648 and 673 K. Since only a small amount of $TiH_{1.971}$ transforms into $TiH_{1.5}$ during the measurement under this condition, the curves show one flat plateau at each temperature. The hydrogen pressures of the absorption plateaus are 1.70 MPa at 673 K, 1.10 MPa at 648 K and 0.57 MPa at 623 K. The hydrogen pressures of the desorption plateaus are 1.47 MPa at 673 K, 0.85 MPa at 648 K and 0.49 MPa at 623 K. From these data, the Van't Hoff Plots (ln *P* vs. 1/*T*) for both

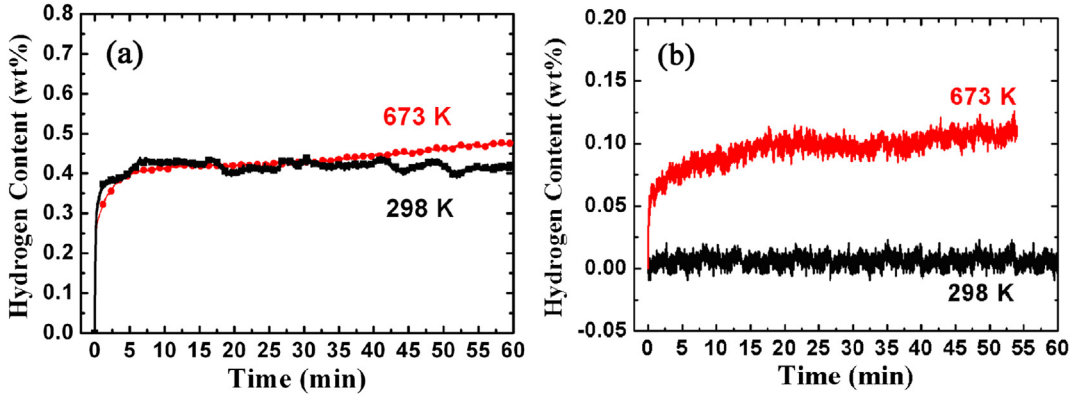

Fig. 9. Hydrogen absorption curves of the $TiH_{1.971}$–$TiH_{1.5}$ nanoparticles under 4 MPa hydrogen pressure (a) and desorption curves under 100 Pa hydrogen pressure at 298 and 673 K (b).

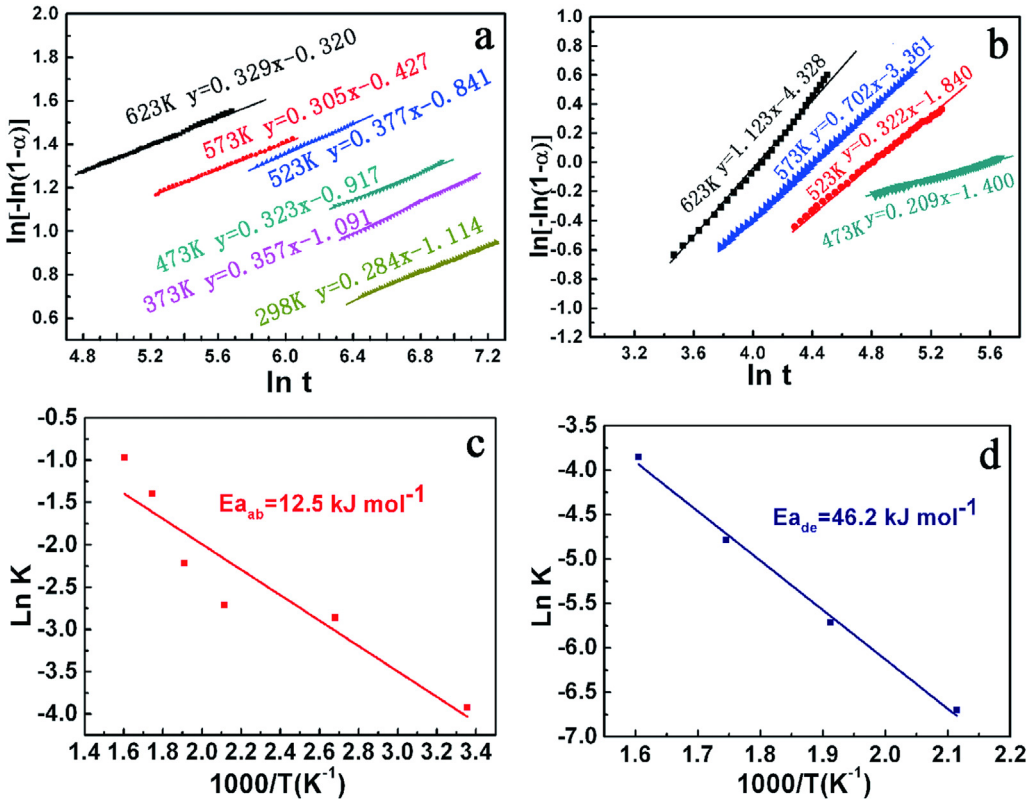

Fig. 10. Plots $\ln(-\ln(1-\alpha))$ vs. $\ln(t)$ for the hydrogenation (a) and dehydrogenation (b) of the Mg–$TiH_{1.971}$–$TiH_{1.5}$ nanocomposite; absorption plot (c) and desorption plot (d) of $\ln k$ vs. $1000/T$ of the Mg–$TiH_{1.971}$–$TiH_{1.5}$ nanocomposite.

absorption and desorption of the Mg–$TiH_{1.971}$–$TiH_{1.5}$ nanocomposite are built in Fig. 12(b). According to the fitting line from the experimental data, the Van't Hoff equation obtained for the absorption is $\ln(P) = -9.18/T + 18.81$ and the goodness of linear fit is 0.986. The obtained value of the formation enthalpy (ΔH_{ab}) for the Mg–$TiH_{1.971}$–$TiH_{1.5}$ nanocomposite is −76.3 kJ mol^{-1}, which is comparable to the standard enthalpy for MgH_2 (~−75 kJ mol^{-1} H_2) [37,40,41]. The Van't Hoff equation for desorption is $\ln(P) = -9.14/T + 18.57$. The decomposition enthalpy (ΔH_{de}) for the Mg–$TiH_{1.971}$–$TiH_{1.5}$ nanocomposite is evaluated to be 76.0 kJ mol^{-1} and the goodness of linear fit is 0.999. This implies that the $TiH_{1.971}$–$TiH_{1.5}$ nanoparticles do not alter the thermodynamics of the sorption process, although they strongly improve the sorption kinetics. Lu and coworkers reported that the calculated reaction enthalpy of the ball-milled MgH_2–$0.1TiH_2$ composite is 68.2 kJ mol^{-1} H_2 [26], lower than that of the standard value for MgH_2 (75 kJ mol^{-1} H_2). They claimed that TiH_2 formed an alloy or solid solution with MgH_2 during the ball milling. In our study, the

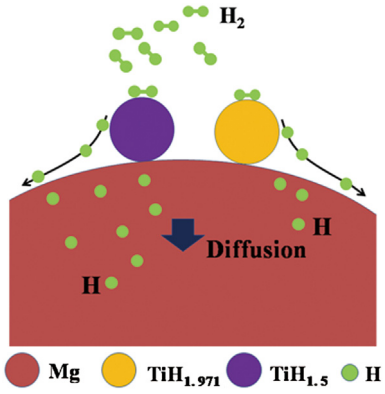

Fig. 11. The illustration of the synergic catalytic effect of the $TiH_{1.971}$–$TiH_{1.5}$ nanoparticles.

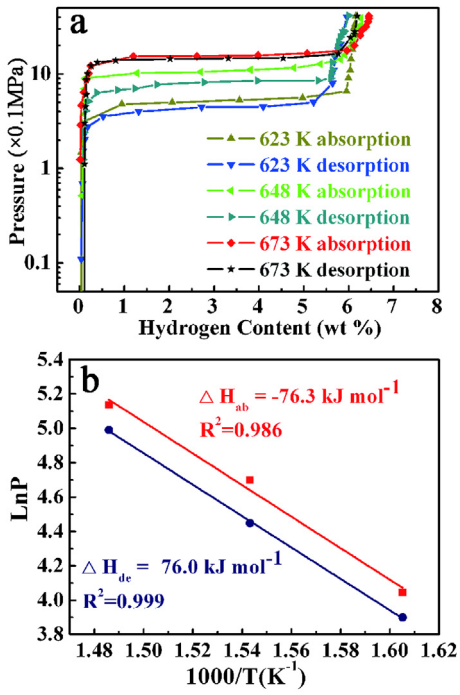

Fig. 12. *P–C* isotherm curves at 623, 648 and 673 K (a) and Van't Hoff plots (b) for the Mg–$TiH_{1.971}$–$TiH_{1.5}$ nanocomposite.

ball milling is not applied, so the $TiH_{1.971}$–$TiH_{1.5}$ nanoparticles cannot form an alloy or solid solution with MgH_2. Thus, the enthalpy reduction for dehydrogenation is not obtained. The Mg–$TiH_{1.971}$–$TiH_{1.5}$ nanocomposite with high sorption kinetics and storage capacity, and low hydrogenation temperature, is a promising candidate for hydrogen storage.

4. Conclusions

The Mg–9.2wt%$TiH_{1.971}$–3.7wt%$TiH_{1.5}$ nanocomposite was successfully prepared by HPMR and hydrogenation/dehydrogenation at 673 K. The Ti hydrides nanoparticles of 13 nm were uniformly dispersed on the surfaces of the Mg nanoparticles of 50–190 nm, and they prevented the Mg nanoparticles from growing during the hydrogenation/dehydrogenation. The Mg–$TiH_{1.971}$–$TiH_{1.5}$ nanocomposite could quickly uptake 4.3 wt% H_2 in 10 min at room temperature and reaches a value of 5.0 wt% in 60 min. The apparent activation energies for hydrogen absorption were calculated to be 12.5 and 46.2 kJ mol^{-1}, respectively. The high sorption kinetics and low activation energy are attributed to the nanostructure of Mg and the synergic effect of $TiH_{1.971}$–$TiH_{1.5}$ nanoparticles.

Acknowledgments

The authors acknowledge the support of this work by the 973 project of MOST of China (No. 2013CB035503), China Program of Magnetic Confinement Fusion under grant number 2012GB102006, the Aeronautical Science Foundation of China (No. 2011ZF51065), and the Scientific Research Foundation for the Returned Overseas Chinese Scholars, State Education Ministry. We also thank Prof. Huiping Duan and Center for Instrumental Analysis and Research, Beihang University for the technical aid in TEM observation.

Appendix A. Supplementary data

Supplementary data related to this article can be found at http://dx.doi.org/10.1016/j.jpowsour.2014.05.066.

References

[1] S. Meng, E. Kaxiras, Z.Y. Zhang, Nano Lett. 7 (2007) 663–667.
[2] F. Cuevas, D. Korablov, M. Latroche, Phys. Chem. Chem. Phys. 14 (2012) 1200–1211.
[3] K.F. Aguey-Zinsou, J.R. Ares-Fernández, Energy Environ. Sci. 3 (2010) 526–543.
[4] D.A. Sheppard, L.H. Jepsen, T.R. Jensen, M. Paskevicius, C.E. Buckley, J. Mater. Chem. A. 1 (2013) 12775–12781.
[5] H.Z. Liu, X.H. Wang, Y.A. Liu, Z.H. Dong, G.Z. Cao, S.Q. Li, M. Yan, J. Mater. Chem. A. 1 (2013) 12527–12535.
[6] W.Y. Li, C.S. Li, H. Ma, J. Chen, J. Am. Chem. Soc. 129 (2007) 6710–6711.
[7] G. Liang, J. Huot, S. Boily, A. Van Neste, R. Schulz, J. Alloys Compd. 292 (1999) 247–252.
[8] S. Rousselot, M.-P. Bichat, D. Guay, L. Roué, J. Power Sources. 175 (2008) 621–624.
[9] G. Krishnan, G. Palasantzas, B.J. Kooi, Appl. Phys. Lett. 97 (2010) 261912.1–261912.3.
[10] G. Liang, J. Huot, S. Boily, A. Van Neste, R. Schulz, J. Alloys Compd. 291 (1999) 295–299.
[11] H.Y. Shao, J. Matsuda, H.Y. Li, E. Akiba, A. Jain, T. Ichikawa, Y. Kojima, Int. J. Hydrogen Energy. 38 (2013) 7070–7076.
[12] Y.J. Choi, J. Lu, H.Y. Sohn, Z.Z. Fang, J. Power Sources. 180 (2008) 491–497.
[13] H. Shao, M. Felderhoff, F. Schüth, Int. J. Hydrogen Energy. 36 (2011) 10828–10833.
[14] J. Lu, Y.J. Choi, Z.Z. Fang, H.Y. Sohn, E. Rönnebro, J. Am. Chem. Soc. 132 (2010) 6616–6617.
[15] B.M. Thaddeus, L.M. Joanne, H.B. Lawrence, B. Hugh, K. Linda, Binary Alloy Phase Diagrams, American Society for Metals, 1986.
[16] H.Y. Shao, G.B. Xin, J. Zheng, X.G. Li, E. Akiba, Nano Energy. 1 (2012) 590–601.
[17] R.W.P. Wagemans, J.H. van Lenthe, P.E. de Jongh, A.J. van Dillen, K.P. de Jong, J. Am. Chem. Soc. 127 (2005) 16675–16680.
[18] P.E. Jongh, P. Adelhelm, ChemSusChem. 3 (2010) 1332–1348.
[19] K.J. Jeon, H.R. Moon, A.M. Ruminski, B. Jiang, C. Kisielowski, R. Bardhan, J.J. Urban, Nat. Mater. 10 (2011) 286–290.
[20] K.F. Aguey-Zinsou, J.R. Ares-Fernández, Chem. Mater. 20 (2008) 376–378.
[21] R. Bardhan, A.M. Ruminski, A. Brand, J.J. Urban, Energy Environ. Sci. 4 (2011) 4882–4895.
[22] T. Liu, C.G. Qin, T.W. Zhang, Y.R. Cao, M. Zhu, X.G. Li, J. Mater. Chem. 22 (2012) 19831–19838.
[23] T. Liu, T.W. Zhang, C.G. Qin, M. Zhu, X.G. Li, J. Power Sources. 196 (2011) 9599–9604.
[24] T. Liu, T.W. Zhang, M. Zhu, C.G. Qin, J. Nanopart. Res. 14 (2012) 738–745.
[25] T. Liu, Y.H. Zhang, X.G. Li, Scr. Mater. 48 (2003) 397–402.
[26] J. Lu, Y.J. Choi, Z.Z. Fang, H.Y. Sohn, E. Rönnebro, J. Am. Chem. Soc. 131 (2009) 15843–15852.
[27] A.R. Kennedy, V.H. Lopez, Mat. Sci. Eng. A. 357 (2003) 258–263.
[28] G.F. Kobzenko, A.P. Kobzenko, M.V. Chubenko, V.V. Petʹkov, A.V. Polenur, Int. J. Hydrogen Energy. 20 (1995) 383–386.
[29] A. Zaluska, L. Zaluski, J.O. Ström-Olsen, J. Alloys Compd. 288 (1999) 217–225.
[30] B. Zahiri, M. Danaie, X.H. Tan, B.S. Amirkhiz, G.A. Botton, D. Mitlin, J. Phys. Chem. C. 116 (2012) 3188–3199.
[31] N.S. Norberg, T.S. Arthur, S.J. Fredrick, A.L. Prieto, J. Am. Chem. Soc. 133 (2011) 10679–10681.
[32] T.R. Jensen, A. Andreasen, T. Vegge, J.W. Andreasen, K. Ståhle, A.S. Pedersen, M.M. Nielsen, A.M. Molenbroek, F. Besenbacher, Int. J. Hydrogen Energy. 31 (2006) 2052–2062.
[33] T. He, Z.T. Xiong, G.T. Wu, H.L. Chu, C.Z. Wu, T. Zhang, P. Chen, Chem. Mater. 21 (2009) 2315–2318.
[34] Y.J. Choi, J.W. Choi, H.Y. Sohn, T. Ryu, K.S. Hwang, Z.Z. Fang, Int. J. Hydrogen Energy. 34 (2009) 7700–7706.
[35] A. Karty, J. Grunzweig-Genossar, P.S. Rudman, J. Appl. Phys. 50 (1979) 7200–7209.
[36] M. Pozzo, D. Alfe, Int. J. Hydrogen Energy. 34 (2009) 1922–1930.
[37] V. Bérubéy, G. Radtke, M. Dresselhaus, G. Chen, Int. J. Energy Res. 31 (2007) 637–663.
[38] L.F. Wang, R.T. Yang, Energy Environ. Sci. 1 (2008) 268–279.
[39] A. Andreasen, T. Vegge, A.S. Pedersen, J. Phys. Chem. B. 109 (2005) 3340–3344.
[40] J.F. Stampfer, C.E. Holley, J.F. Suttle, J. Am. Chem. Soc. 82 (1960) 3504–3508.
[41] J.J. Vajo, F. Mertens, C.C. Ahn, R.C. Bowman Jr., B. Fultz, J. Phys. Chem. B. 108 (2004) 13977–13983.